

AN UPDATED WIND TURBINE IMPACT ASSESSMENT METHOD APPLIED TO THE WSR-88D NETWORK

Lindsey Richardson^{a,*}, Autumn Losey-Bailor^a, Jane Krause^{a,b}, Bill Ward^a

^a Radar Operations Center

^b Centuria Corporation

The pursuit of any energy source presents its own challenges, and wind energy in particular has unique, detrimental impacts on weather radar data. As turbine industry standards evolve and wind turbines increase in height and number, ways to assess their impact must be re-examined and updated. This project compares two assessment methods: 1) an existing method that calculates impacts out to designated ranges based on a standard turbine height, and 2) a proposed method that defines impacts based on the number of elevation angles intersected by the project-specific turbine heights. Information from WSR-88D sites is compared with existing wind farm installations as reported in publicly available data to assess potential data impacts.

1. INTRODUCTION

Wind Turbine Clutter (WTC) is currently an unsolved problem regarding any wind turbine within the Radar Line of Sight (RLOS). Existing weather radar clutter filtering techniques were designed using stationary targets such as buildings, but rotating blades create a notable moving target within a radar resolution volume that is challenging to separate from atmospheric signals. The resulting degradation of data impacts both visual analysis and derived algorithm products, which can interfere with the mission of weather radar data to provide accurate, good quality input for weather analysis, warning, and verification. This challenge is increasingly affecting weather radars and meteorological agencies around the world, and the World Meteorological Organization (WMO) has mentioned the critical need for collaboration between radar and wind turbine siting in the "Guide to Meteorological Instruments and Methods of Observation" (WMO 2017). In particular, "WMO encourages national radio agencies to develop acceptable obstruction criteria and to provide tools to help the wind farm developer on site selection."

An earlier study on this topic performed by the United Kingdom Royal Air Force Signals Engineering Establishment (RAFSEE 1994) revealed potential impacts to radar signals and recommended steps be taken to account for wind turbine installations and possible mission

impacts. Almost a decade later, a United States Department of Defense report (DOD 2006) discussed similar impacts and a need for proper assessment and mitigation of wind turbine signatures and installation for different radar missions. Many agencies around the world began using various criteria such as distance from the radar or percentage of blockage to quantify potential impacts from wind turbines (Angulo et al. 2014). By 2007, the Radar Operations Center (ROC) had developed such a method.

The ROC's existing procedure analyzes potential impacts to any nearby Weather Surveillance Radar – 1988 Doppler (WSR-88D) attempting to determine if and where turbines could intersect or interact with a radar beam (Vogt et al. 2007; Burgess et al. 2008; Vogt et al. 2009a; Vogt et al. 2009b; Vogt et al. 2011). Results are then used during coordination between the wind farm developers/operators and the local WFO to alter developments and/or create mitigation strategies. In short, the method compares radar beam height to the total turbine height to find if or where intersections between the turbine and radar beam occur.

Of particular interest from the results is the number of radar elevation angles impacted by WTC. The more angles contaminated by WTC, the more impacts on data and products are visible. Impacts can be classified as No Impact, Low, Moderate, or Significant depending on their location, the number of angles affected, and the number of existing wind turbines surrounding the

*Corresponding Author address: Lindsey M. Richardson, Radar Operations Center, Norman, OK, email: Lindsey.M.Richardson@noaa.gov

AMS 40th Conference on Radar Meteorology 2023

The views expressed are those of the authors and do not necessarily represent those of NOAA or the NWS.

radar. For example, a “Low” impact classification may have turbines that affect only the lowest elevation angle at a location with few or no other nearby wind turbine installations. Because only the lowest angle is contaminated, the second elevation angle and above can be used to continue assessment of weather conditions as they pass through WTC. A “Significant” classification, on the other hand, is bestowed when any turbine impacts three or more elevation angles. Contamination of the lowest three angles effectively eliminates the ability to assess the lowest portion of the atmosphere, where violent weather is most likely. Additionally, blockage and down-range shadowing of lower elevation angles lowers the accuracy of analysis even beyond the extent of WTC. Therefore, accurate representation of the potential WTC impacts is vital for communicating the risk of data contamination.

The following example demonstrates the existing ROC analysis method, a version

established in 2020. Figure 1 highlights the location of the Grandview I wind turbines near KAMA (Amarillo, TX) from the U.S. Wind Turbine Database (USWTDB). The results (Figure 2) place impacts from Grandview I outside of all impact classification zones, meaning the turbines should have no impact on the RLOS. Figure 3 shows the associated reflectivity and velocity on a day without weather in a relatively standard atmosphere. Information from the Long-Term Average Reflectivity (LTAR) product in Figure 4 shows how the signature is persistently visible at this radar, and how the signal can have downstream shadow effects on the data. Despite the existing analysis suggesting the turbines would not be visible (No Impact), the base data and derived products show consistent impacts (Low Impact). This indicates that something about the existing analysis procedure is inaccurately capturing the estimated impacts of wind turbine installations.

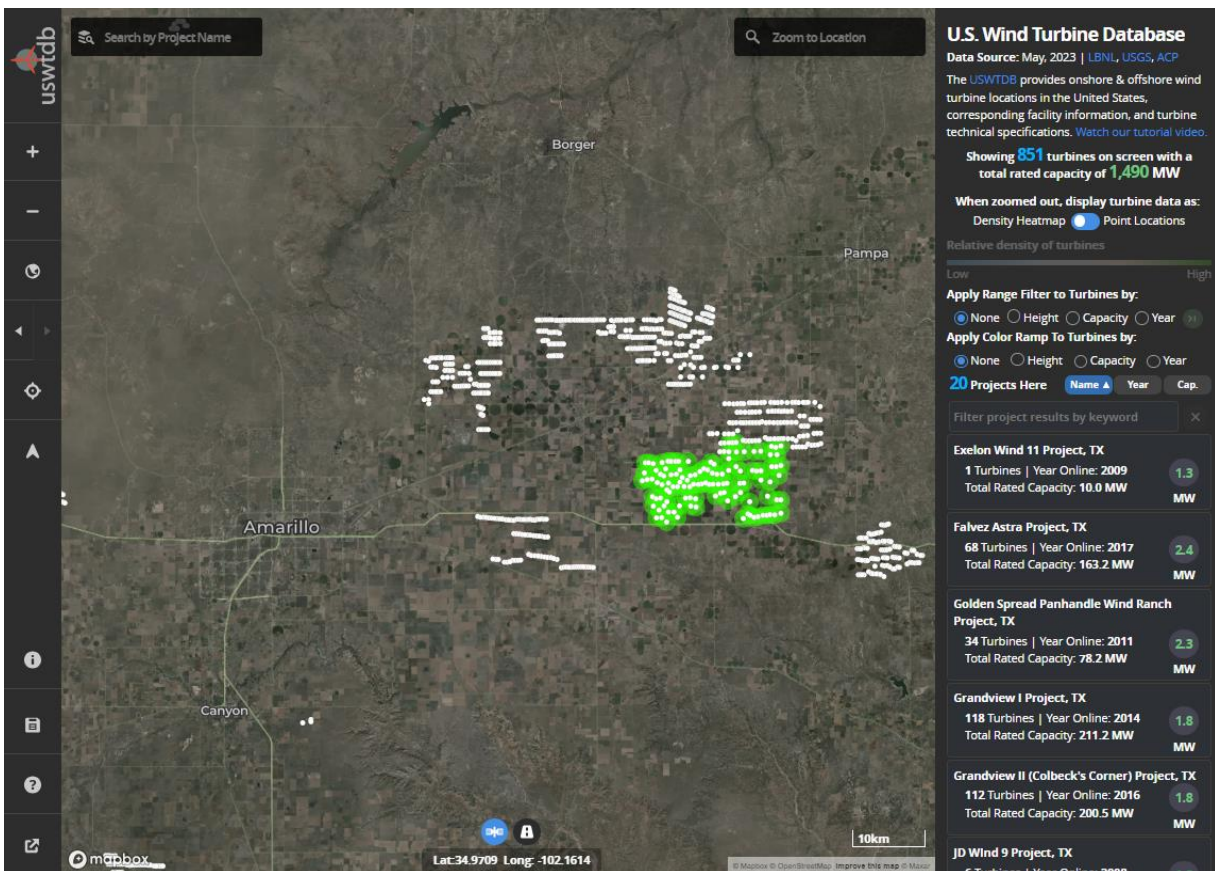


Figure 1: Locations of the Grandview I wind turbines east of Amarillo, TX are highlighted in green in the USWTDB web page.

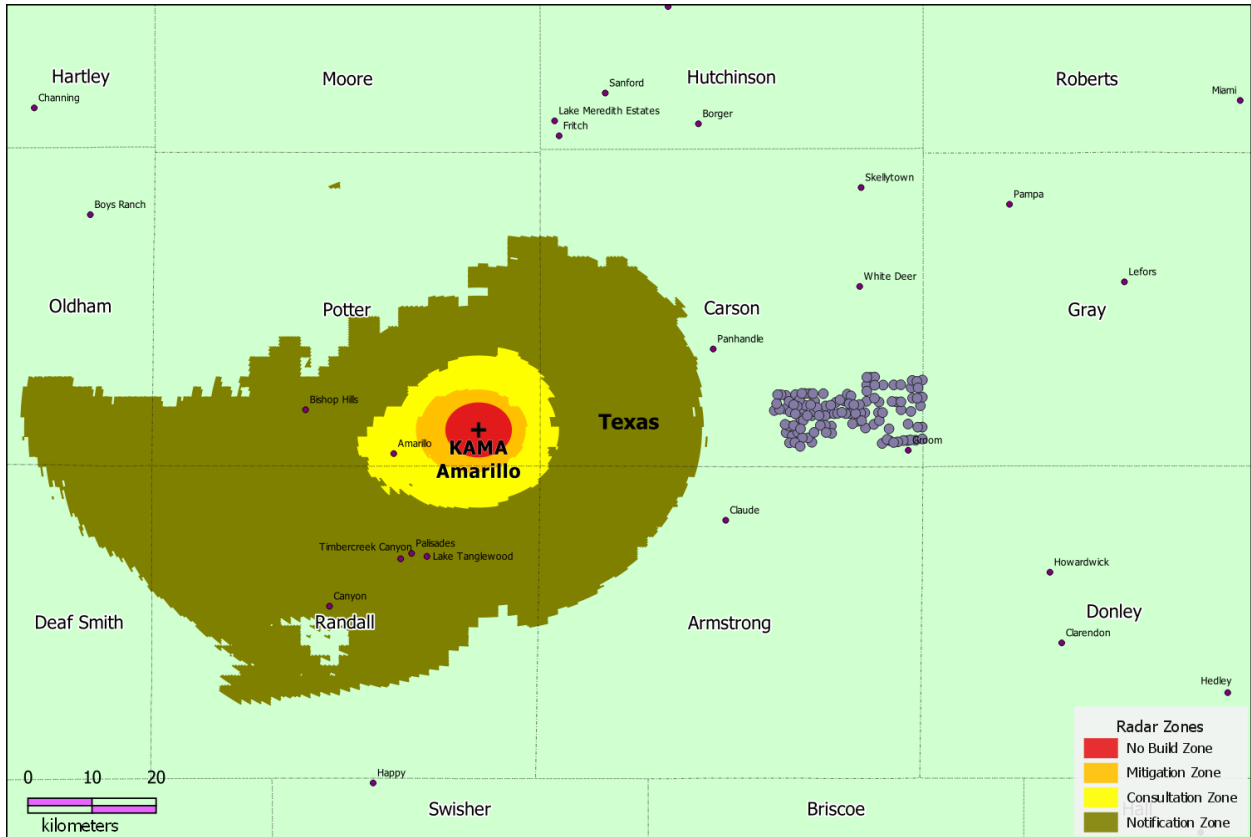


Figure 2: Results from the existing ROC analysis procedure suggesting the Grandview I turbines are outside of any of the colored impact regions.

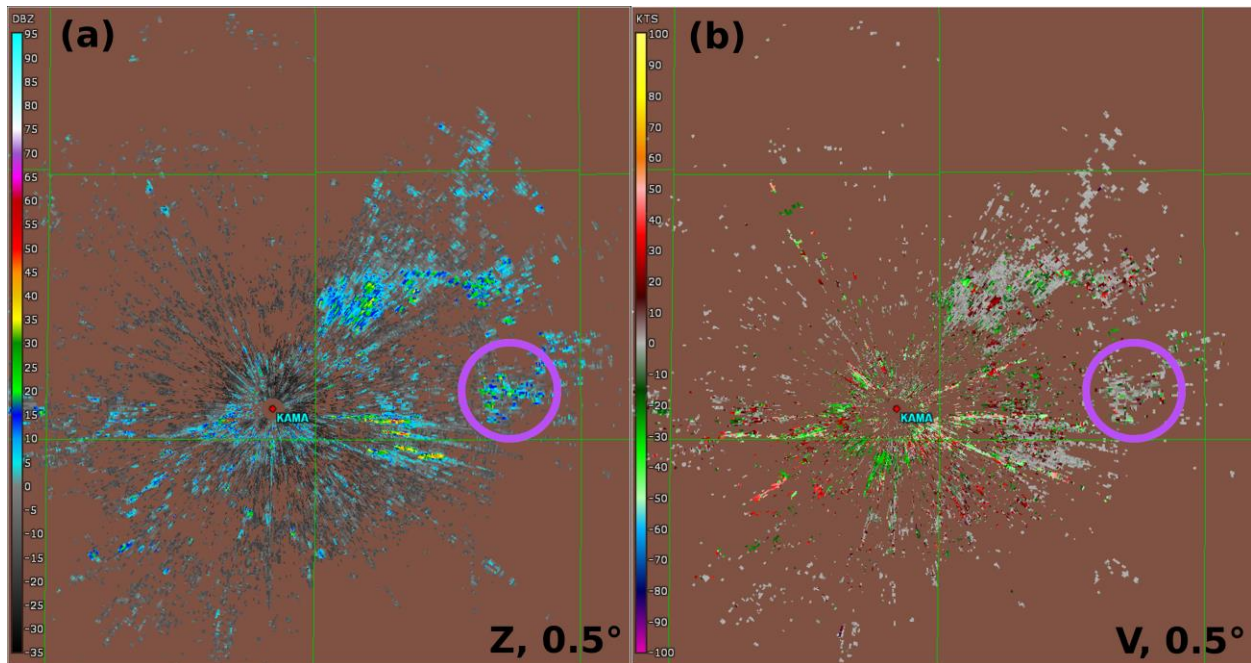


Figure 3: KAMA reflectivity (a) and velocity (b) data from 0.5° on 20230107 at 17:04 UTC showing wind turbine clutter in base moments, including the Grandview I turbines (circled).

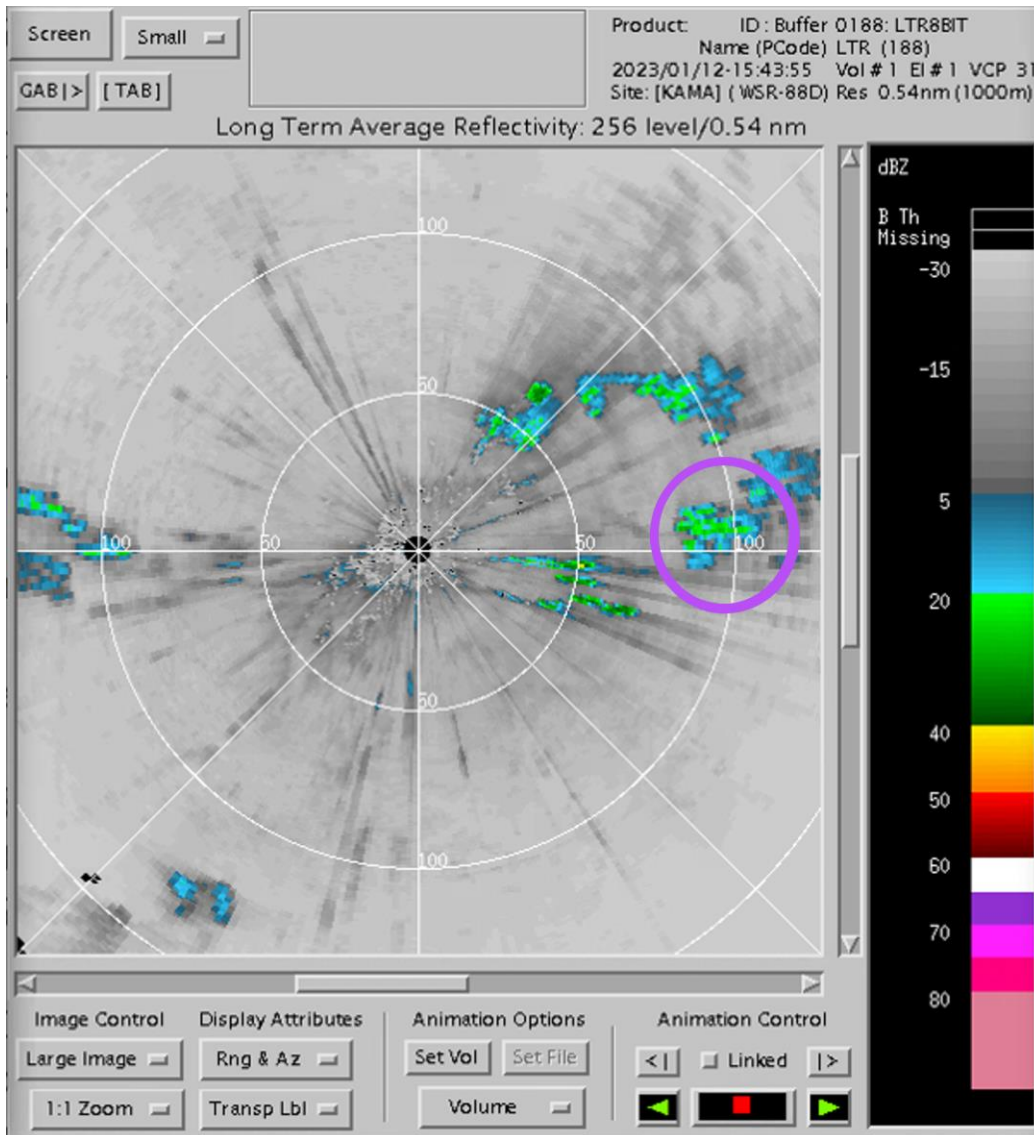


Figure 4: LTAR image from 30 days of data collection at KAMA showing persistent clutter residuals from wind turbines. Returns associated with Grandview I are circled. Image provided by Dave Smalley, MIT Lincoln Laboratory.

To check the performance of the method, maps of WSR-88D RLOS are compared to existing wind turbine installations as reported by the USWTDB v5.3 (Hoen et al. 2018) and the Federal Aviation Administration (FAA) Obstruction Evaluation/Airport Airspace Analysis (OE/AAA) database (CGH Technologies, Inc. 2022). All possible entries from the USWTDB are considered. From OE/AAA, items classified as "Off-Airport" from the regions of "WTW" (Wind Turbine West) and "WTE" (Wind Turbine East) are also considered. The OE/AAA entries were filtered further to exclude airborne, tethered, and

off-shore installations. While there are installations of wind turbines in Alaska, Hawaii, Puerto Rico, and Guam, as well as non-U.S. locations, the bulk of new installation proposals is occurring within the Contiguous United States (CONUS), which will be the focus for this study. In order to improve impact estimates seen in operational WSR-88D data, a detailed reanalysis of the physical factors in the existing method is explored. Radar beam and wind turbine features are considered for physical accuracy of the method, as well as additional radar antenna pattern characteristics.

2. ANALYSIS FACTORS

2.1 Radar Factors

A WSR-88D scans the atmosphere using a rotating, parabolic dish. Scans normally rotate in sweeps of 360° in azimuth at a specific elevation angle. Elevation angles operationally vary from -0.2 to +19.5°, and a specific defined sequence of elevation sweeps denotes a Volume Coverage Pattern (VCP; NOAA 2017). Thus, a rotating beam of energy is transmitted, and reflected energy off of targets in the RLOS is received. The path this energy takes varies based on atmospheric conditions that can be difficult to quantify, hence the common assumption of a Standard Atmosphere in height estimations. In a Standard Atmosphere, the radar beam will increase in Above Radar Level (ARL) height with increasing distance due to the curvature of the Earth. The actual ARL height will vary based on the terrain at the given location, so terrain information within the RLOS must also be considered. A coverage map of the radar beam characteristics can be used to determine if a structure, such as a wind turbine, would be visible to the radar during normal operational modes.

The Center of Beam (COB) height formula related to the radar site (s) in ARL units used in the WSR-88D is shown in Eq. 1:

$$COB_s = (r * \sin(\theta)) + \frac{r^2}{2 * k * a} \quad (1)$$

where r is the range from the radar in kilometers, θ is the elevation angle, k is the refractive index factor, and a is the radius of the earth in kilometers (WSR-88D ROC 2020; Gao et al. 2006). Constant values of $a = 6371$ km and $k = 1.21$ are used for all WSR-88D sites.

To get the Mean Sea-Level (MSL) form requires the height from the ground to the top of

the tower for the radar site (h_{ts}), height from the top of the tower to the feedhorn (h_f) where the energy would be transmitted and received, and the height of the MSL terrain elevation at the base of the radar site tower (h_{e_s}).

Terrain can vary drastically over the RLOS, so it is crucial to have the beam height relative to the terrain elevation at a given point in range. We can determine the Above Ground Level (AGL) height at a given range by subtracting out the associated MSL terrain elevation at the location (h_{e_r}) seen in Eq 2.

$$COB_r = COB_s + h_{ts} + h_f + h_{e_s} - h_{e_r} \quad (2)$$

Values for h_{ts} , h_f and h_{e_s} come from the metadata for a given site (WSR-88D ROC 2022). All WSR-88Ds use a consistent pedestal size and antenna setup, giving a constant h_f value of 4.7 m. Terrain elevation for each point in range (h_{e_r}) is calculated as the maximum value from either the National Elevation Dataset (NED; USGS 2022) or the Shuttle Radar Topography Mission (SRTM; NASA and NGA 2000) 1-arc second data. Information from the NED is prioritized, but SRTM data are used to fill in any missing locations.

Because radar beams broaden as they travel in range, the Bottom of Beam (BOB) height changes in relation to the beamwidth (θ_B) as shown in Eq. 3.

$$BOB_r = COB_r - \left(\frac{\theta_B * r}{2} \right) \quad (3)$$

Figure 5 visualizes the terms and shows how a change in terrain can put turbines into the RLOS. Any structure below the BOB_r height is considered outside of the approximate beam, so a structure would have little to no impact on the beam.

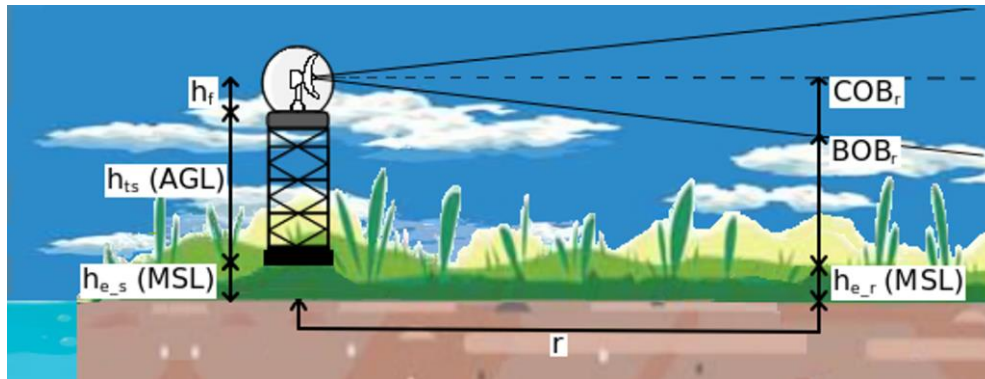


Figure 5: Diagram of MSL and AGL relationships for WSR-88D beam height calculations.

θ_B is often set to the one-way half-power beamwidth (HPBW), corresponding to the 3-dB beamwidth. WSR-88Ds use a parabolic dish with angular symmetry, so the HPBW can be estimated with Bessel functions or from an approximated form because the beamwidth is relatively small as mentioned in Doviak and Zrnić (1993). Resulting HPBW values are within 0.01° between the two equations. WSR-88Ds use the approximated form for beamwidth (Doviak and Zrnić Eq. 3.2b, repeated here as Eq. 4):

$$\theta_B = \frac{1.27 * \lambda}{D} \quad (4)$$

where λ is the wavelength and D is the antenna diameter. The antenna diameter for all WSR-88Ds is 8.544 m (28 ft), but the frequency ($\lambda \setminus c$) ranges from 2700-3000 MHz depending on the site. As such, the largest operational θ_B is approximately 0.95° . This value was used to estimate BOB_r for all WSR-88Ds because it would cover the largest possible standard main beam for any location. Originally, the method used a 1.0° beamwidth for all sites (Vogt et al. 2011), but it was updated to use 0.95° circa 2015.

For each WSR-88D, a map of radar range bins is created for each 0.1° in azimuth and 0.25 km in range out to 300 km. This 300 km limit is slightly over 60% of the maximum range of the WSR-88D – results of the early RAFSEE study suggested that projects within this range should be presented for impact analysis (RAFSEE 1994, DOD 2006). Beyond this range, the height of the beam is estimated to be well above a non-mountainous surface. Additionally, 300 km corresponds to the existing Doppler and Dual-Polarization data range limit.

The COB_r and BOB_r are calculated for each point for the main set of angles associated with VCP 12 (WSR-88D ROC 2022), which covers the angles for most operational WSR-88D scanning strategies. Some sites have lower starting elevation angles referred to as Base Tilts that are also considered. The analysis considers a site's first elevation angle as their lowest operational angle – for sites with Base Tilts, this angle is lower than the standard 0.48 degrees. For example, KTYX (Ft. Drum, NY) uses the standard 0.48, 0.88, and 1.31° as the first three elevation angles while KBUF (Buffalo, NY) uses 0.31, 0.48, and 0.88° as the first three elevation angles. Accounting for site-specific angles helps

ensure accurate representation of possible impacts seen during normal field operations.

Specific Zones are mapped out for each of the three lowest operational elevation angles related to their BOB_r , with one additional zone defined for critical impacts and safety:

- 1) Notification Zone – Impacts only the first elevation angle
- 2) Consultation Zone – Impacts up to the second elevation angle
- 3) Mitigation Zone – Impacts up to the third elevation angle
- 4) No Build – A hard defined limit in range, currently set at 4 km

Layers for each zone are created in increments of 10 m from 100 to 400 m AGL. The visual representation of impacts can be shown by using zone layers close to the height of a wind turbine (within 10 m).

2.2 Wind Turbine Factors

Once the radar coverage is established, it can then be used to determine if external structures intersect the beam. The majority of wind turbine installations in the United States are Horizontal-Axis Wind Turbines consisting of a tower, a hub for equipment and rotor, and a number of blades to capture horizontal winds for movement (Wilburn 2011; Wass 2018). Radar energy is reflected off of each surface, which contributes to non-standard electromagnetic travel paths commonly called multi-pathing (Kent et al. 2008; Isom et al. 2009; Ohs et al. 2010; Leijnse et al. 2022). Rotating blades are known to reflect radar beams towards the surface, back to the blade, and then back to the radar. Energy can also creep around the portions of the structure and cause a variety of shadowing effects (RAFSEE 1994; ANF 2005; DOD 2006; Isom et al. 2009; Greving et al. 2012; Norin 2015). Studies such as the one by Norin (2015) also suggest the possibility of receiving returns in the reflectivity and Doppler spectrums from dust and downstream turbulence. Such effects will mostly be included in the same affected radar range gate as other wind turbine impacts, so no additional extension around the turbine location is considered.

There are two main factors that make up a height impact from a wind turbine: the turbine tower height up to the rotor (AGL), and the blade length. The tower/hub height is the AGL height up to the location of the rotational axis. The full

vertical impact of a wind turbine is modified by the length of the blade when aligned vertically with its tower. This inclusive vertical height is considered the total turbine height (h_{tt}) that could impact the airspace (Figure 6). Other sources

may refer to this as the “blade tip height”, but this paper will consistently use “total turbine height” to avoid confusing this term with the “blade length”.

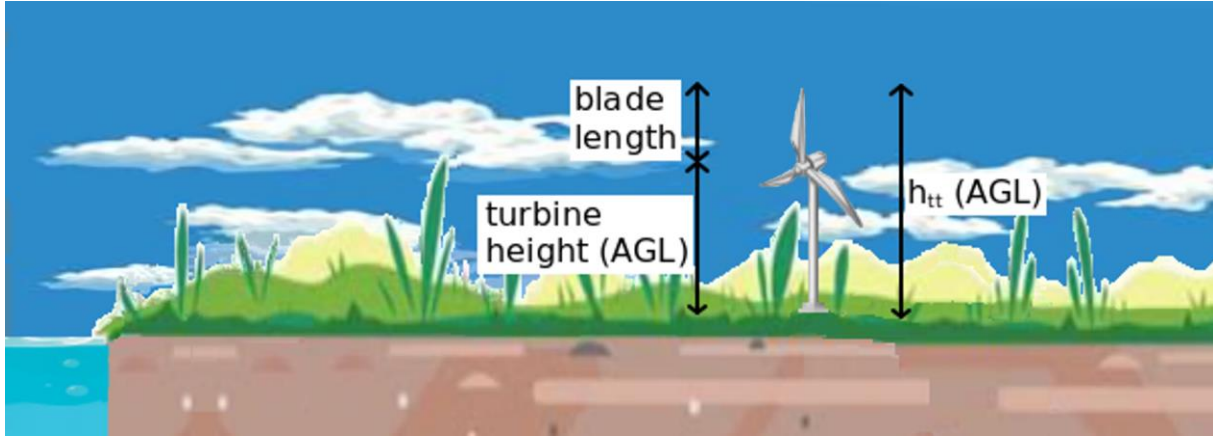


Figure 6: AGL height parameters associated with a Horizontal-Axis Wind Turbine.

When considering an impact to the RLOS, the total turbine height is the most critical for analysis because while the height to the hub could impact a number of elevation angles, the full extent of the blades could impact additional elevation angles. It is noted that blade orientation to the beam can also modify the impacts from a wind turbine (e.g., Beauchamp and Chandrasekar 2017; Leijnse et al. 2022); rotating blades are a non-constant blockage target and blade orientation can move with the wind. Despite these known factors, the ROC method does not use blade diameter in the analysis because the ROC often does not receive the blade length or diameter from the developer.

A value for the Meters Into the Beam (MIB) is used to determine if a turbine would be visible from a standard beam (Eq. 5).

$$MIB = h_{tt} - BOB_r \quad (5)$$

The ROC analysis method originally assumed a standard total turbine height to relate the impact zones to specific range limits (Vogt et al. 2011), but the standard turbine height has increased over time. Figure 7 demonstrates that the median has exceeded 160 meters since 2020. The databases used to create Figure 7 include entries from small individual turbines to large commercial farms, which gives a wide range of heights. The boxes represent the 25th and 75th percentiles (1st and 3rd quartile), with the purple line representing the median (50th percentile, 2nd quartile). Furthermore, Figure 8 reveals a rapid increase in installation since 2017. Figure 9 maps out this increase in taller towers across the CONUS with snapshots from 2012, 2017, and 2022. These findings may correspond with studies suggesting improvements to efficiency and power output with turbine height (e.g., Lantz et al. 2019). Using the appropriate total turbine height values related to an actual turbine project is crucial for accurately representing MIB and determining the number of elevation angles impacted.

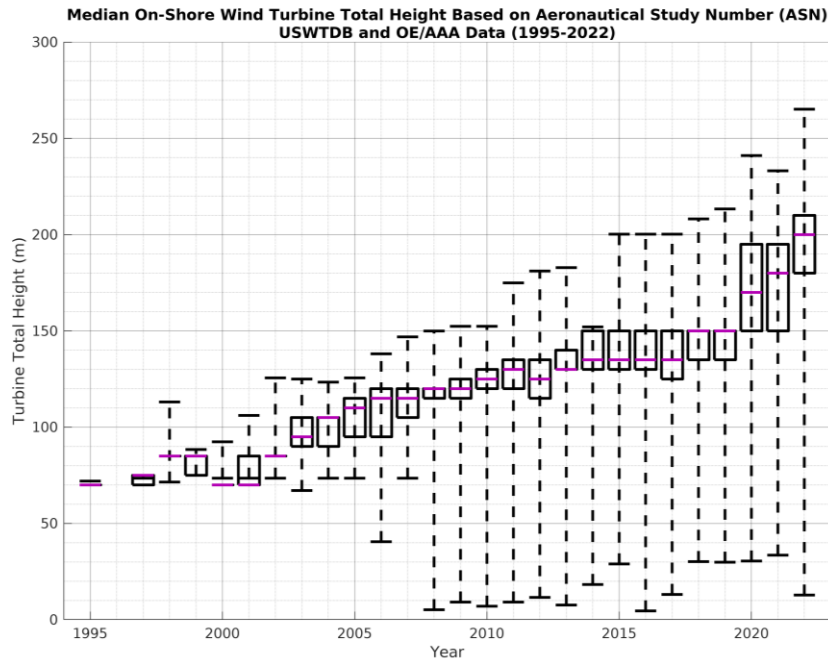


Figure 7: Box and whisker plot of Total Turbine Height sorted by year based on the ASN showing the full min and max range as well as the quartiles. Medians are highlighted in purple.

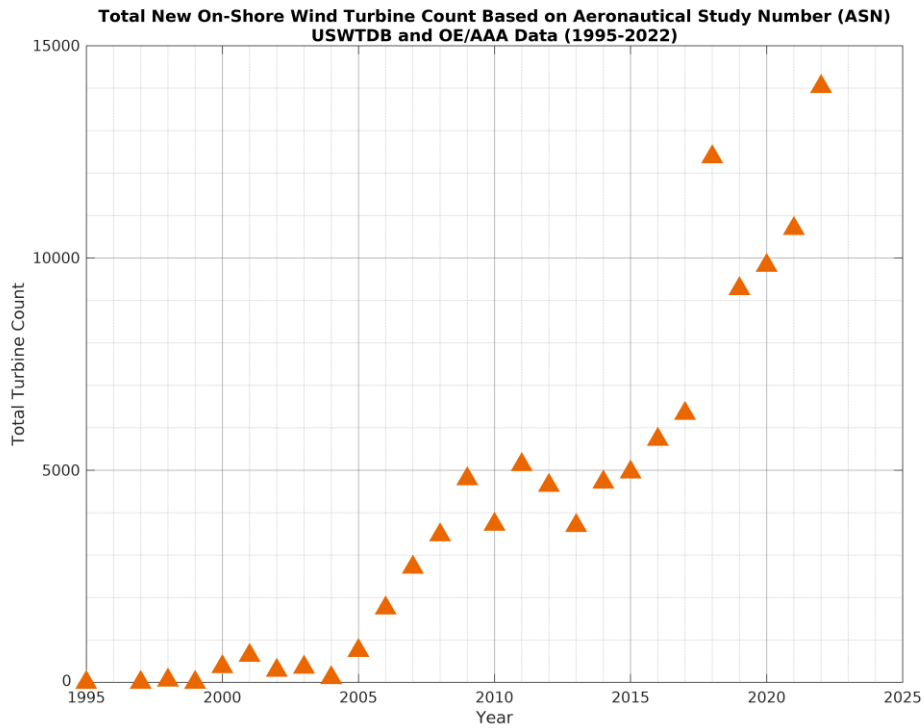


Figure 8: Total count of wind turbine entries per year based on ASN.

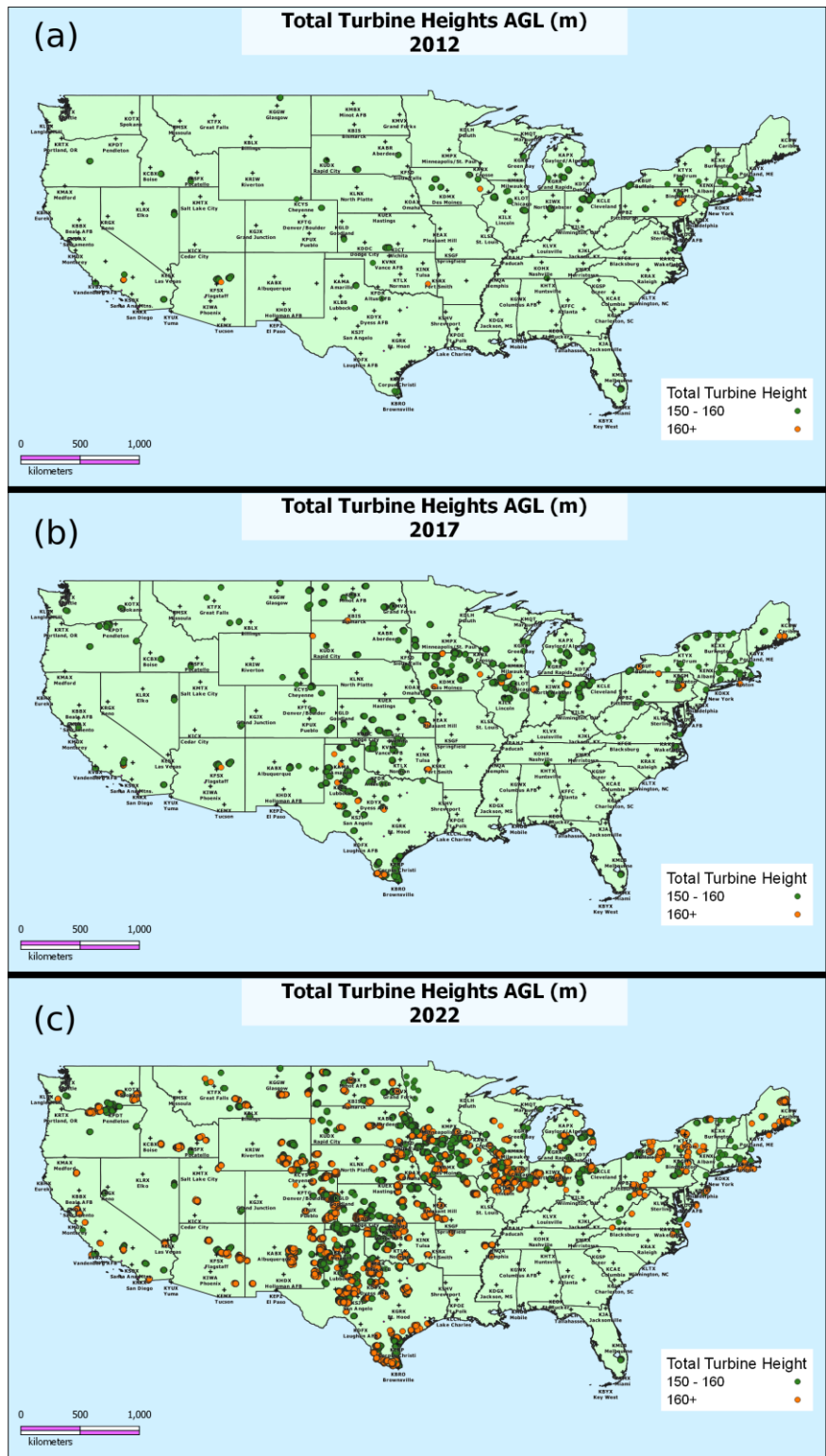


Figure 9: Relative distribution of wind turbine locations across the CONUS with total turbine heights between 150-160 meters (green circles) and greater than 160 meters (orange circles). Turbines with heights below 150 meters not shown.

One factor not yet considered by the existing method is potential for contamination from sidelobes. According to the FMH-11 Part B, the WSR-88D has a first sidelobe level at -29 dB and will get returns when there is a reflectivity gradient exceeding 40 dB/° sustained over $\sim 2^\circ$ compared to the main lobe represented by the HPBW (NOAA 2005). Sidelobe returns are an annulus around the main beam, so effects can come from the sides, above, or below the main beam. For a procedure relying on the estimated BOB height, any extension below this could be contributing to returns as long as the power is strong enough. Sidelobe contamination from wind turbines has been noted in studies such as Isom et al. (2009) and Norin (2015). Figure 10 shows an example of reflectivity returns and the

azimuthal gradient over $\sim 2^\circ$ from the Cimarron I and Cimarron II wind turbines northwest of KDDC (Dodge City, KS) on 20221206 at 22:09:01 UCT as a B-scan plot of the first elevation angle (0.5°). Reflectivity values range between 20-60 dBZ, and there are several areas where the gradient exceeds 30-40 dB/°. Thus, it is likely that the wind turbine clutter is being picked up as part of sidelobe power returns. Such a strong gradient is unsurprising in clear weather. Sidelobe contamination may have a chance to be reduced in strong weather returns, but it is not guaranteed, especially in weather situations such as snow, the edge of a squall line, or the edge of a supercell (Figures 11-13).

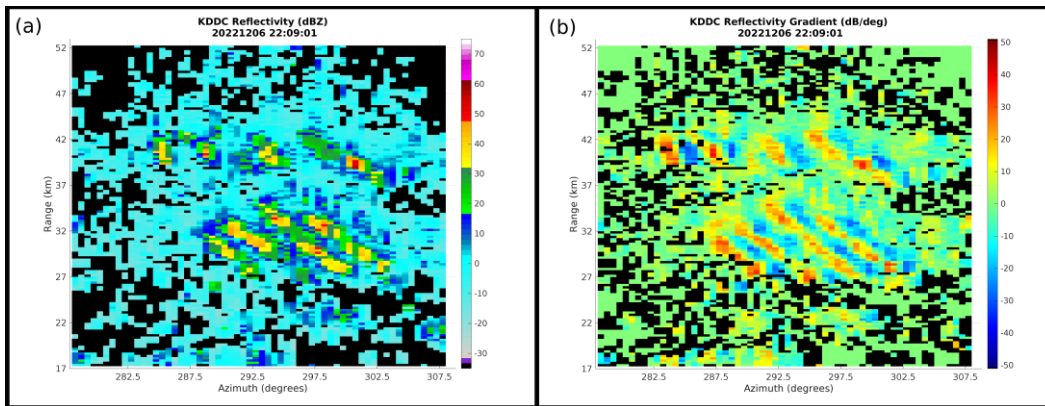


Figure 10: Reflectivity and associated gradient in azimuth across wind turbine returns.

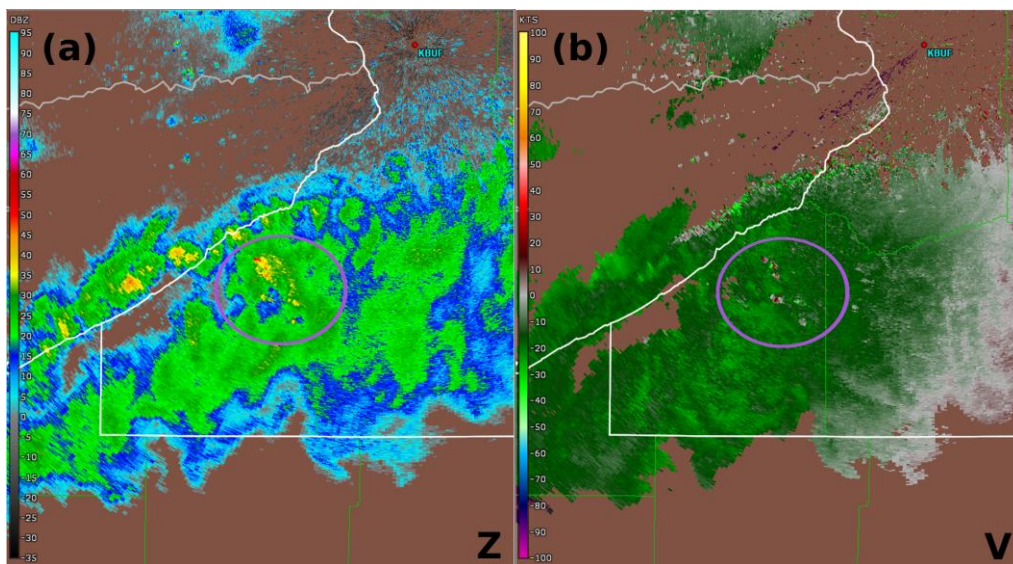


Figure 11: KBUF Z and V data from 0.5° on 20221117 at 06:07 UTC showing wind turbine clutter in a snow squall characterized by high reflectivity values and spurious velocity signatures.

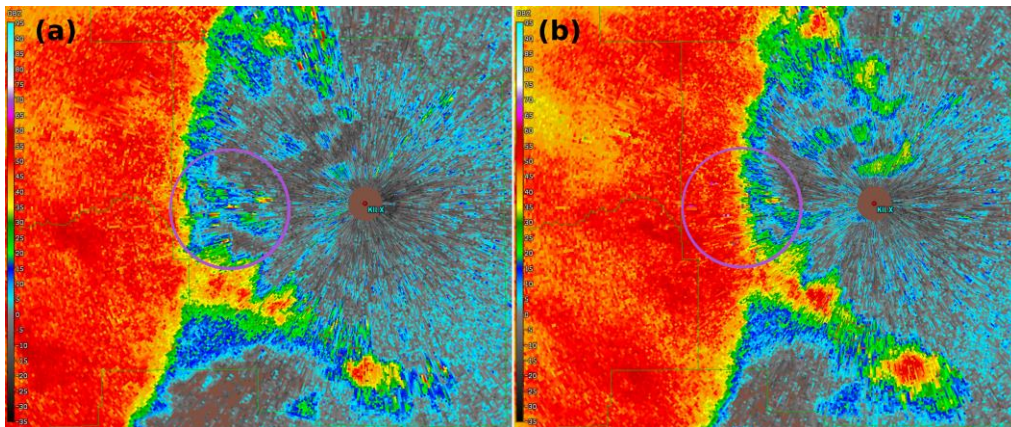


Figure 12: KILX Z data from 0.5° 20230629 at 17:15 UTC (a) and 17:19 UTC (b). Spots of high reflectivity are present even when the strong thunderstorm is over the wind farm.

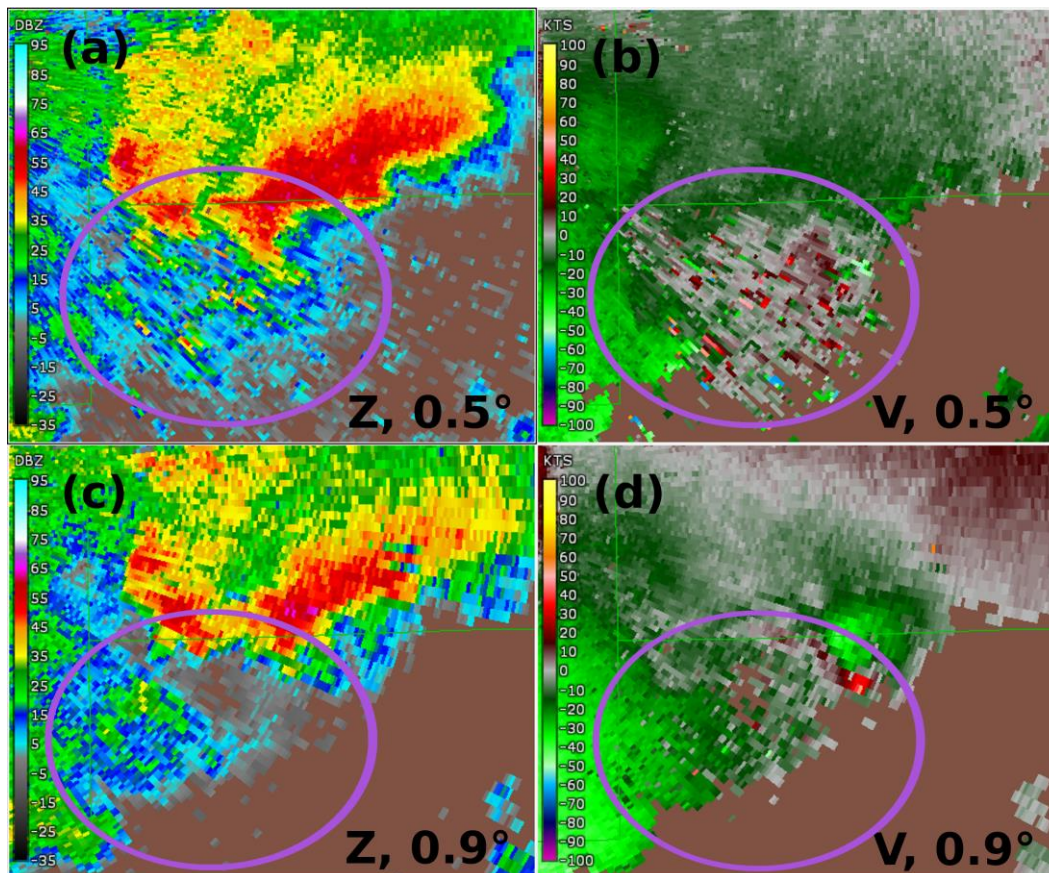


Figure 13: KILX Z and V data from 0.5° and 0.9° on 20181202 at 00:30 UTC as a tornado-warned supercell crosses through an area with wind farms. The signature is lost completely at 0.5°, and is still contaminated and unclear at 0.9°.

Because sidelobe contamination corresponds with the radar detecting wind turbines in an area broader than the standard beam, it could be an important factor missing from the existing method that affects the estimation for the BOB height. For the WSR-88D, if the HPBW is 0.95° as previously established, the first sidelobe (-29 dB) is around 1.31° . This First Sidelobe Beamwidth (FSBW) can be used as the value of θ_B in Eq. 3 to assist with capturing potential impact from wind turbines. Figure 14 shows the approximate BOB difference between using the HPBW and the FSBW. It is a slight adjustment downward, but there remains a point in range where a turbine would not be visible even to this extended beamwidth under normal atmospheric conditions.

3. USING UPDATED PARAMETERS

Revisiting the Grandview I case from Figure 2, the analysis procedure is reprocessed using the FSBW value and total turbine height to adjust the impact zone areas. Figure 15 shows the extension of the zone related to the first elevation angle (Notification Zone) due to the broader beamwidth being closer to the ground. This extension of the zone more closely matches the reflectivity returns seen in Figure 3. The results from this case would change from a classification of No Impact to Low Impact due to its continual presence in the first elevation angle data.

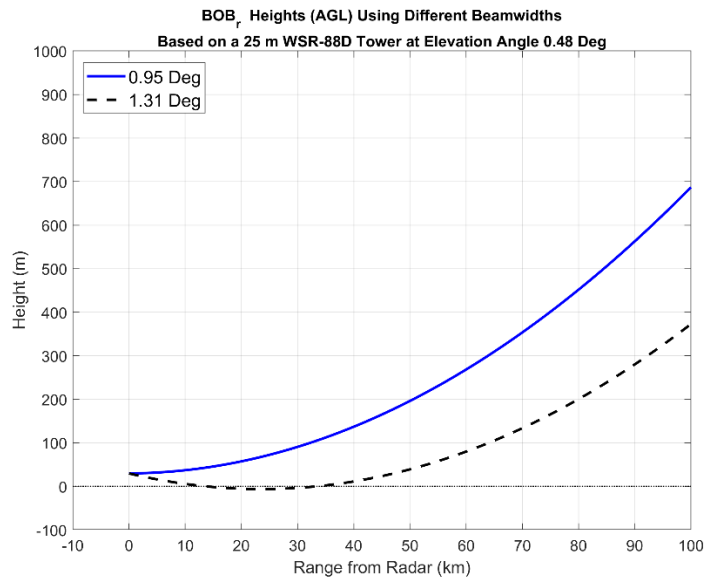


Figure 14: BOB height difference between using the HPBW and FSBW.

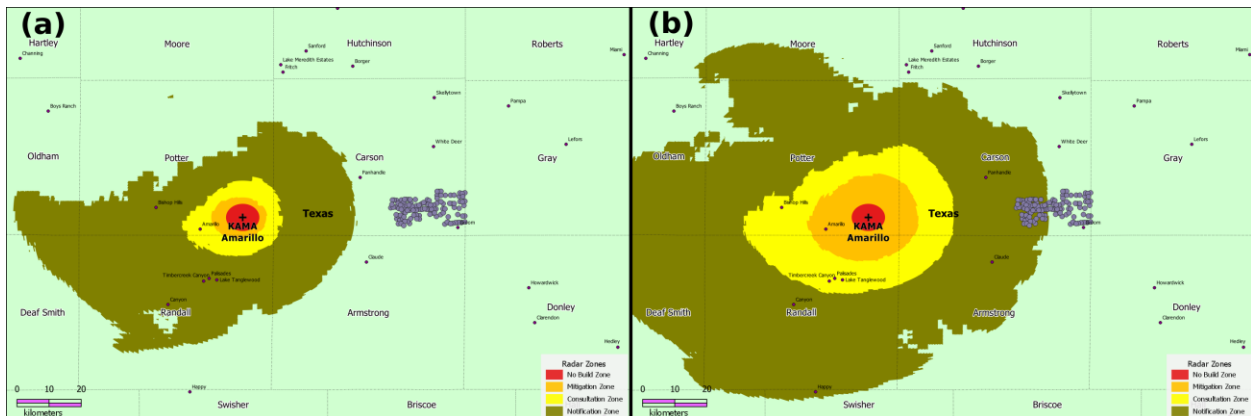


Figure 15: ROC wind turbine impact analysis results for Grandview I wind turbines using a standard HPBW (a) and the FSBW (b).

Next is an example of a case with potential impacts to multiple elevation angles (Figure 16). The original analysis procedure for the Wilton Wind Farm near KBIS (Bismarck, ND) suggests the turbines would only have potential impacts in the first elevation angle. Using the FSBW suggests the towers would actually have residuals in the second elevation angle (Consultation Zone). Figure 17 shows the reflectivity and velocity data from KBIS on 20221201 at 18:14:23 UTC when the weather

was clear. Panels (a) and (b) are from the 0.5° elevation angle, while panels (c) and (d) are from the 0.9° elevation angle. Strong power returns and variable velocity returns north of Bismarck near the county line match the location of the Wilton Wind Farm. There are fewer returns in total area at the second elevation angle compared to the first, yet contamination is still present. Thus, the FSBW correctly captures the chance for clutter effects on the additional elevation angle.

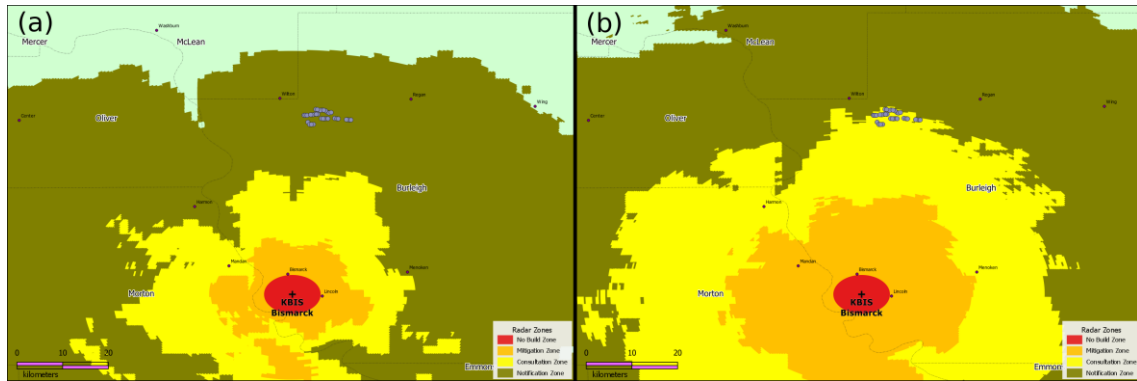


Figure 16: ROC wind turbine impact analysis results for Wilton Wind Farm using a standard HPBW (a) and the FSBW (b).

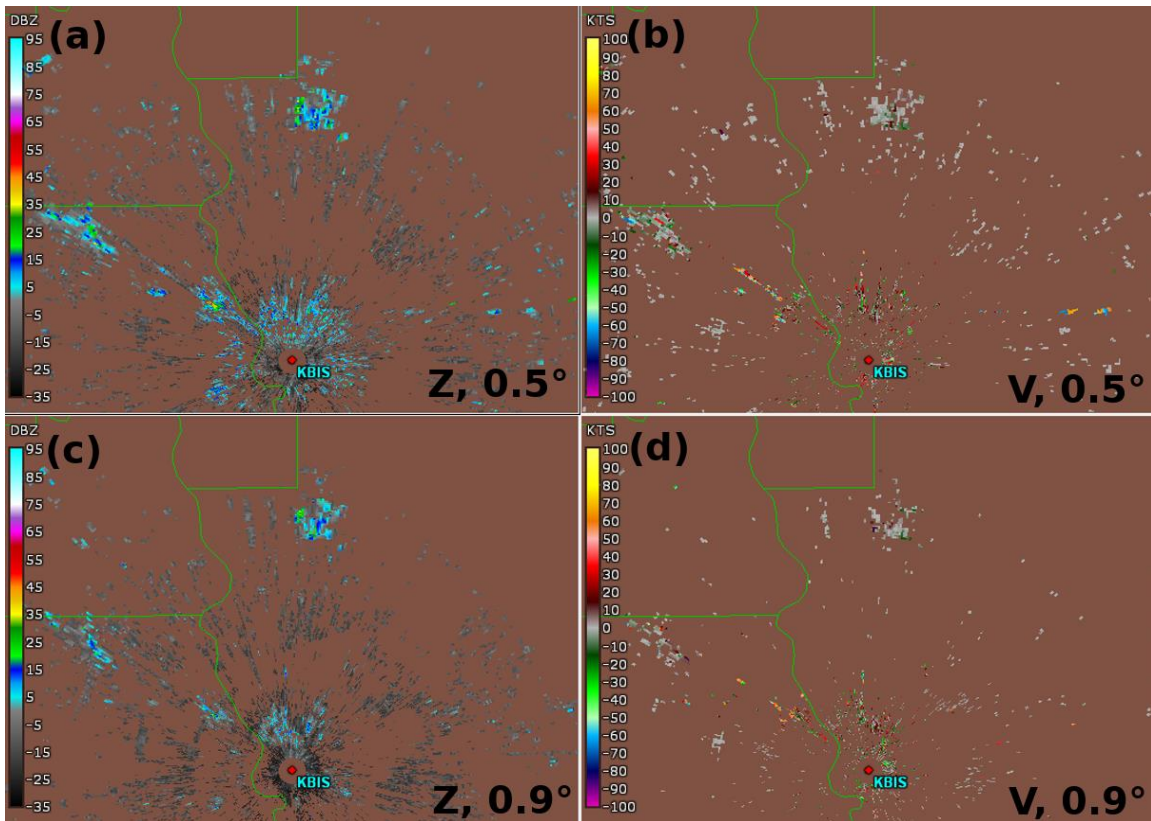


Figure 17: KBIS Z and V data from 0.5° and 0.9° on 20221201 at 18:14 UTC showing the Wilton Wind Farm turbines at multiple elevation angles.

Because the only change to the method is a slight extension of the beamwidth, it should not extend impact areas to places without them. Figure 18 shows how the Wildcat I wind farm is considered No Impact in both the original and updated procedure. This is verified with the reflectivity and velocity data from KIND (Indianapolis, IN) in Figure 19. Similarly, Figure

20 shows how the Notrees Wind Farm near KMAF (Midland/Odessa, TX) could impact the first elevation angle when using the standard HPBW or the FSBW. The updated procedure does not suggest impacts to any additional angles, which can be verified visually in the reflectivity and velocity data in Figure 21.

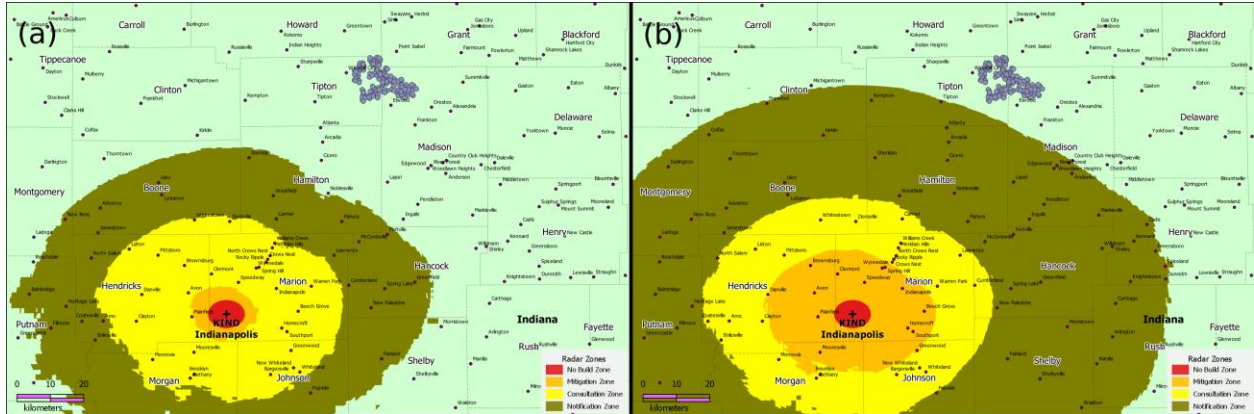


Figure 18: ROC wind turbine impact analysis results for Wildcat I wind turbines using a standard HPBW (a) and the FSBW (b).

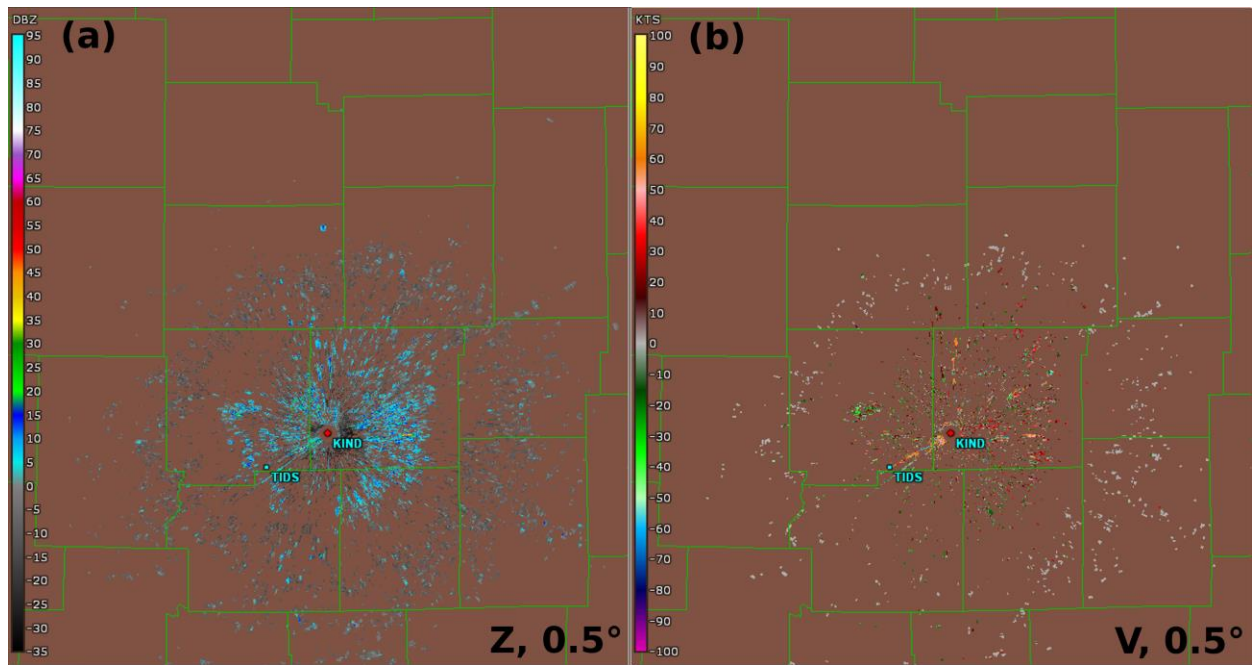


Figure 19: KIND Z and V data from 0.5° on 20221218 at 15:40 UTC showing no wind turbine clutter from the Wildcat I turbines.

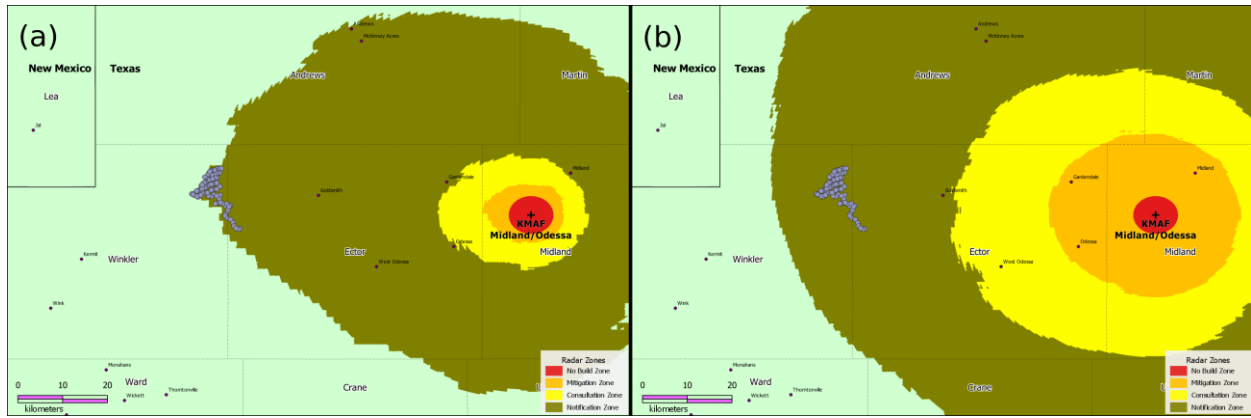


Figure 20: ROC wind turbine impact analysis results for Notrees wind turbines using a standard HPBW (a) and the FSBW (b).

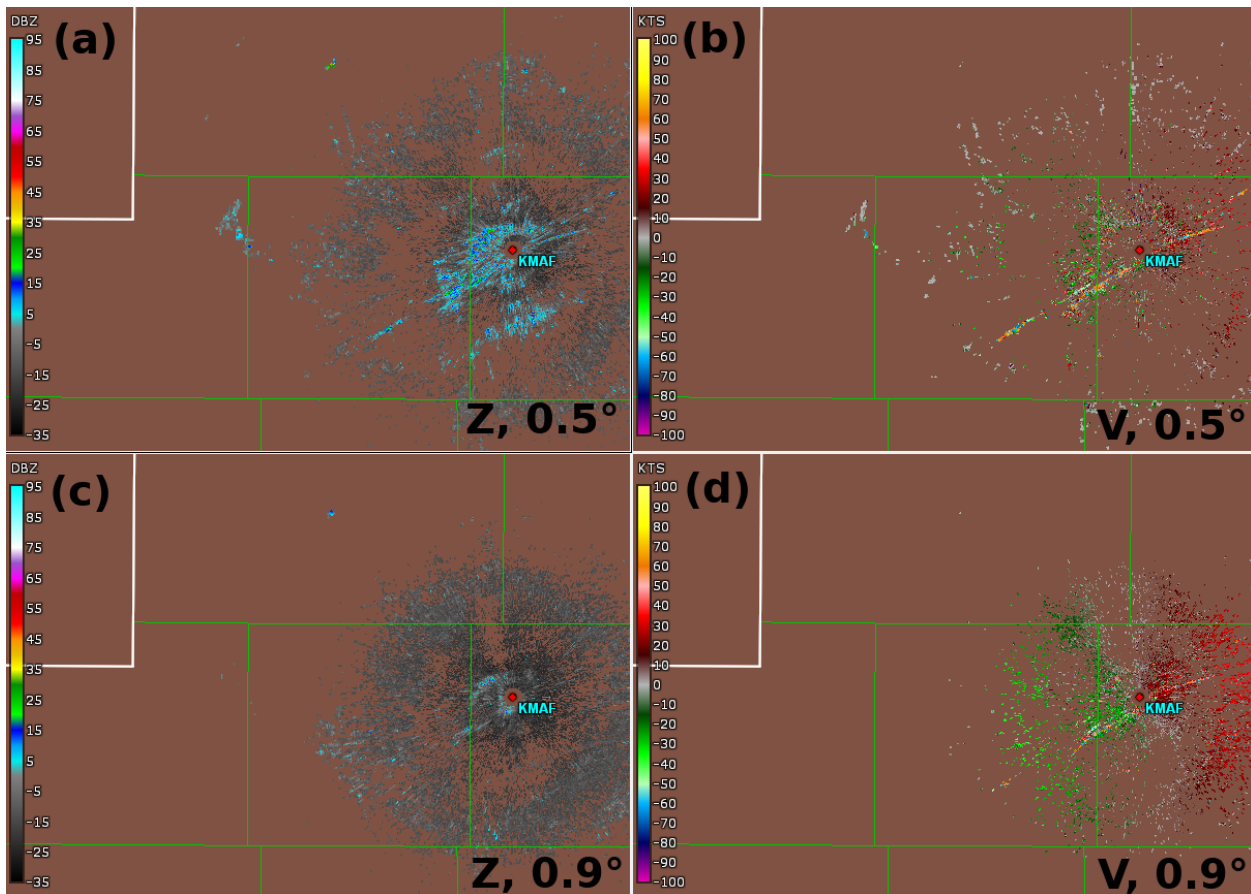


Figure 21: KMAF Z and V data from 0.5° and 0.9° on 20221231 at 17:00 UTC showing the Notrees wind turbines only at 0.5°.

4. SUMMARY

Increased installation of wind turbines has also increased the contamination of radar data due to structures built within the RLOS. Wind turbine contamination is difficult or impossible to remove from the original signal while retaining the true weather signal. Accurate estimation of wind turbine impacts to weather radar missions is critical for meteorological institutions in order to facilitate discussions with wind farm developers regarding mitigation strategies. These strategies could involve altering placement or height of the most impactful turbines, or adjusting turbine rotation rules during critical weather events such as severe thunderstorms, tornadoes, and heavy snow squalls. The Radar Operations Center has been using a basic method for estimating impacts to WSR-88D systems based on the total number of angles impacted at a given radar site.

In order to create adequate impact estimation procedures, various properties of the radar and of wind turbine structure must be considered. Radar factors include beam propagation, atmospheric assumptions, physical operating characteristics, and coverage related to surrounding terrain. Wind turbine factors include the axis orientation type, general materials and models used, and the possibility for the height to be extended by the blades. Comparing the height of the radar beam to the full height of the wind turbine has shown to be a reasonable estimate for potential impacts to radar data. Cases where the wind turbine intersects the beam under standard atmospheric conditions have the highest potential to be a constant contaminant that would impact data quality of visual analysis and derived products such as precipitation estimation.

The existing ROC analysis procedures (2020 version) do not account for one major

factor – the significant returns from sidelobes, especially the first sidelobes. Using the sidelobes as an approximation of a broader beamwidth accounts for the chance to retrieve the information closer to the ground, which translates to the additional chance for having wind turbine contamination in the radar data. Test cases estimating impacts to the RLOS were performed using the beamwidth related to the first sidelobe level in the height calculations instead of the standard Half Power Beamwidth. Results show increased accuracy of locations with potential impacts without excessively extending the classification horizontally in range or vertically to additional elevation angles. Even so, this updated method may not capture all possible impacts under every condition; for example atmospheric conditions such as ducting can show WTC at elevations and ranges outside the analysis results.

The best solution to avoid impacts to weather radar missions remains to build wind turbines outside of the RLOS. Figure 22 overlays WSR-88D impact zones onto the National Renewable Energy Laboratory (NREL) projections of average wind speed at common wind turbine heights (Weber et al. 2021). Based on this, many locations outside of WSR-88D RLOS areas are available to explore for wind energy production. For other cases and proposals requesting development closer to a radar, it is recommended to use a procedure that accounts for as many potential impacts as possible. The use of the FSBW has shown to be relevant for WSR-88D analysis, and may be a useful factor to consider for other weather radar systems as we continue attempting to balance a variety of energy sources with weather missions.

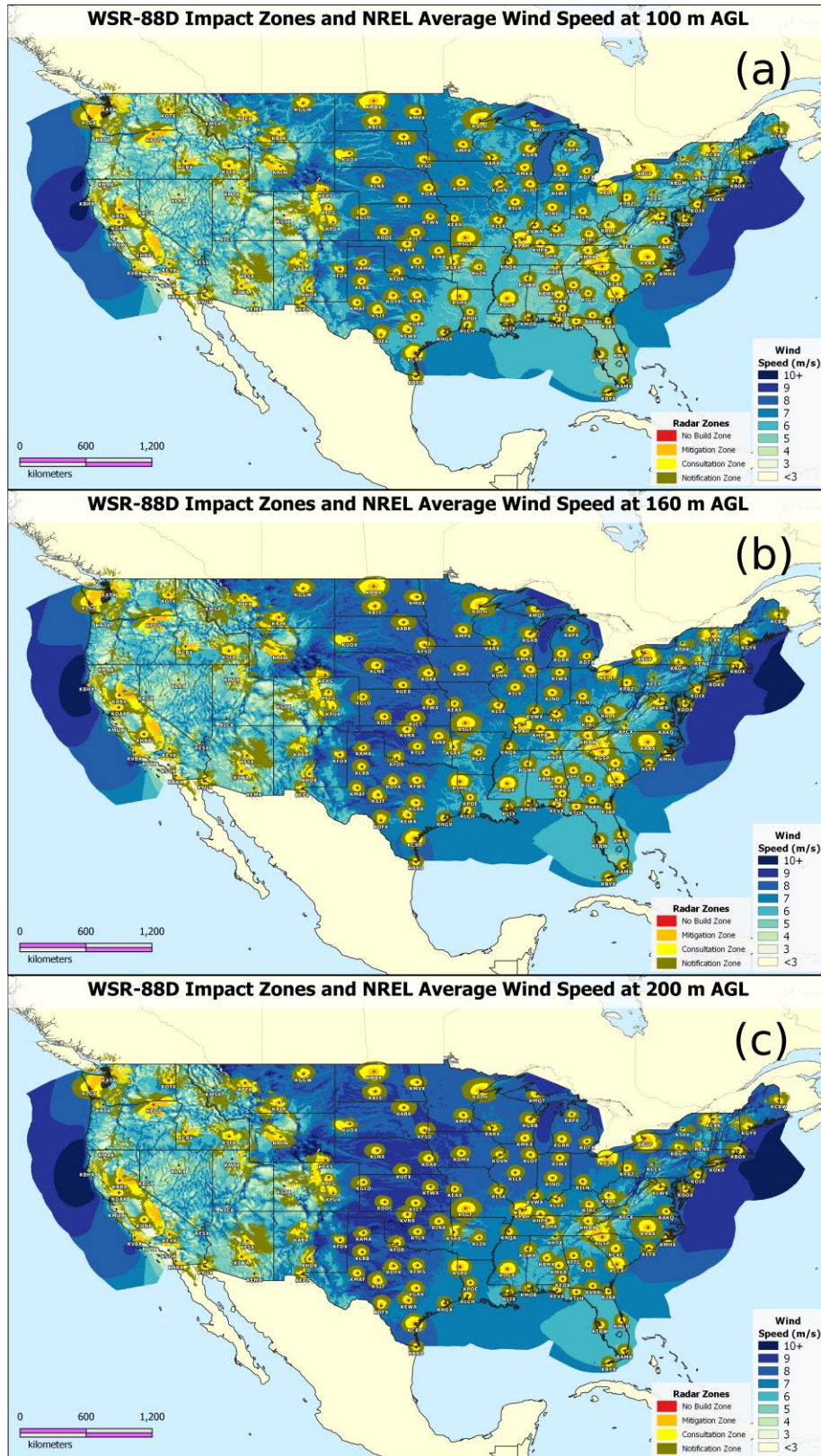


Figure 22: WSR-88D impact zone coverage and average wind speeds over the CONUS showing many areas with the potential for wind energy collection with a variety of tower heights beyond the RLOS.

5. REFERENCES

ANF, 2005: Perturbations du fonctionnement des radars meteorologiques par les eoliennes, Technical Report Rapport CCE5 No.1, Commision Consultative de la Compatibilité Electromagnétique, <https://www.anfr.fr/fileadmin/mediatheque/documents/etudes/Rapport%20perturbations%20%20fonctionnement%20radars%20meteorologiqu es%20par%20eoliennes.pdf>. (In French)

Angulo, I., D. De La Vega, I. Cascón, J. Cañizo, Y. Wu, D. Guerra, and P. Angueira, 2014: Impact analysis of wind farms on telecommunication services. *Renewable and Sustainable Energy Reviews*, **32**, 84-99, <https://doi.org/10.1016/j.rser.2013.12.055>.

Beauchamp, R. M. and V. Chandrasekar, 2017: Suppressing Wind Turbine Signatures in Weather Radar Observations. *IEEE Transactions on Geoscience and Remote Sensing*, **55**, No. 5, 2546-2562, <https://doi.org/10.1109/TGRS.2016.2647604>.

Burgess, D. W., T. D. Crum T. D., and R. J. Vogt, 2008: Impacts of wind farms on WSR-88D radars. Preprints, *24th Int. Conf. on Interactive Information Processing Systems (IIPS) for Meteorology, Oceanography, and Hydrology*, New Orleans, LA, Amer. Meteor. Soc., 6B.3, <http://ams.confex.com/ams/pdfpapers/128810.pdf>.

CGH Technologies Inc., 2022: Obstruction Evaluation/Airport Airspace Analysis (version 2022-NOV.7). FAA, accessed on February 21, 2023, <https://oeaaa.faa.gov/oeaaa/external/public/publicAction.jsp?action=showCaseDownloadForm>.

DOD, 2006: Report to the Congressional Defense Committees, The Effect of Windmill Farms on Military Readiness, 62 pp, <https://www.acq.osd.mil/dodsc/library/Congressional%20Report%20Impact%20of%20Wind%20Turbines%202006%20AFRL.pdf>.

Doviak, R. J., and D. S. Zrnić, 1993: *Doppler Radar and Weather Observations*. 2nd ed. Dover Publications, 562 pp.

Gao, J., K. Brewster, and M. Xue, 2006: A comparison of the radar ray path equations and approximations for use in radar data assimilations. *Adv. Atmos. Sci.*, **23**, 190-198, <https://doi.org/10.1007/s00376-006-0190-3>.

Greving, G., W. D. Biermann, and R. Mundt, R., 2012: Wind turbines as distorting scattering objects for radar—visibility, desensitization and shadowing. *Proceedings, 13th International Radar Symposium*, 275-277.

Hoen, B.D., J. E. Diffendorfer, J. T. Rand, L. A. Kramer, C. P. Garrity, H. E. and Hunt, 2018: United States Wind Turbine Database v5.3 (Jan 1, 2023). U.S. Geological Survey, American Clean Power Association, and Lawrence Berkeley National Laboratory data release, <https://doi.org/10.5066/F7TX3DN0>.

Isom, B. M., and Coauthors, 2009: Detailed Observations of Wind Turbine Clutter with Scanning Weather Radars. *J. Atmos. Oceanic Technol.*, **26**, 894-910, <https://doi.org/10.1175/2008JTECHA1136.1>.

Kent, B.M., K.C. Hill, A. Buterbaugh, G. Zelinski, R. Hawley, L. Cravens, Tri-Van, C. Vogel, and T. Coveyou, 2008: Dynamic radar cross section and radar Doppler measurements of commercial General Electric windmill power turbines Part 1: Predicted and measured radar signatures. *IEEE Antennas and Propagation Magazine*, **50**, No 2., 211-219, <https://doi.org/10.1109/MAP.2008.4562424>.

Lantz, E. J., J. O. Roberts, J. Nunemaker, E. DeMeo, K. L. Dykes, and G. N. Scott, 2019: Increasing Wind Turbine Tower Heights: Opportunities and Challenges. Golden, CO, National Renewable Energy Laboratory, NREL/TP-5000-73629, 65 pp., <https://doi.org/10.2172/1515397>.

Leijnse, H., R. Teschl, H. Paulitsch, F. Teschl, G. Holmes, and L. F. Sidselrud, 2022: OPERA-4: On the coexistence of weather radars and wind turbines, 63 pp, https://www.eumetnet.eu/wp-content/uploads/2022/08/OPERA_wind_turbine_report_20220225.pdf.

NASA and NGA, 2000, Shuttle Radar Topography Mission 1 Arc-Second Global Data

Set, U.S. Geological Survey database, accessed December 19, 2022, at <https://doi.org/10.5066/F7PR7TFT>

NOAA, 2005: Doppler Radar Meteorological Observations: Part B – Doppler Radar Theory and Meteorology. Federal Meteorological Handbook No. 11, FCM-H11B-2005, 219 pp., <https://www.icams-portal.gov/resources/ofcm/fmh/FMH11/fmh-11B-2005.pdf>.

NOAA, 2017: WSR-88D Meteorological Observations: Part C – WSR-88D Products and Algorithms. Federal Meteorological Handbook No. 11, FCM-H11C-2017, 396 pp., <https://www.icams-portal.gov/resources/ofcm/fmh/FMH11/fmh11partC.pdf>.

Ohs, R.R., G. J. Skidmore, and G. Bedrosian, 2010: Modeling the effects of wind turbines on radar returns. Proceedings, *2010-MILCOM 2010 MILITARY COMMUNICATIONS CONFERENCE*, San Jose, CA, IEEE, 272-276, <https://doi.org/10.1109/MILCOM.2010.5680316>.

USGS, 2022, National Elevation Dataset 1 Arc-Second Digital Elevation Model, U.S. Geological Survey National Map 3DEP Downloadable Data Collection, accessed December 19, 2022, at <https://prd-tnm.s3.amazonaws.com/index.html?prefix=StagedProducts/Elevation/1/>.

Vogt, R.J., J. R. Reed, T. Crum, J. T. Snow, R. Palmer, B. Isom, and D. W. Burgess, 2007: Impacts of wind farms on WSR-88D operations and policy considerations. Preprints, *23rd Int. Conf. on Interactive Information Processing Systems (IIPS) for Meteorology, Oceanography, and Hydrology*, San Antonio, TX, Amer. Meteor. Soc., 5B.7, https://ams.confex.com/ams/87ANNUAL/techprogram/paper_120352.htm.

Vogt, R. J., T. D. Crum, J. B. Sandifer, R. Steadham, T.L. Allmon, G. Secrest, E.J. Ciardi, R. Guenther, R. Palmer, 2009a: Continued Progress in Assessing and Mitigating Wind Farm Impacts on WSR-88Ds. Preprints, *25th Int. Conf. on Interactive Information Processing Systems (IIPS) for Meteorology, Oceanography, and Hydrology*, Phoenix, AZ, Amer. Meteor. Soc.,

Paper 11B.6, <https://ams.confex.com/ams/pdfpapers/150646.pdf>.

Vogt, R. J., T.D. Crum, J. B. Sandifer, E. J. Ciardi, and R. Guenther, 2009b: A way forward, wind farm – weather radar coexistence. Preprints, *WINDPOWER 2009, American Wind Energy Association Conference and Exhibition*, Chicago, IL, https://www.roc.noaa.gov/WSR88d/Publicdocs/WindPower2009_Final.pdf.

Vogt, R. J., T. D. Crum, W. Greenwood, E.J. Ciardi, R.G. Guenther, 2011: New Criteria for Evaluating Wind Turbine Impacts on NEXRAD Radars. Preprints, *WINDPOWER 2011, American Wind Energy Association Conference and Exhibition*, Anaheim, CA, https://www.roc.noaa.gov/wsr88d/PublicDocs/WINDPOWER2011_Final.pdf.

Wass, R., 2018: Design of Wind Turbine Tower Height and Blade Length: an Optimization Approach. B.S. thesis, Dept. of Mechanical Engineering, The University of Arkansas, 76 pp, <https://scholarworks.uark.edu/meeguht/70>.

Wilburn, D.R., 2011: Wind energy in the United States and materials required for the land-based wind turbine industry from 2010 through 2030. U.S. Geological Survey Scientific Investigations Report 2011–5036, 22 pp, <http://pubs.usgs.gov/sir/2011/5036>.

WMO, 2017: Guide to Meteorological Instruments and Methods of Observation. 2014 Edition, updated in 2017. Geneva, Switzerland, World Meteorological Organization, WMO No. 8, 1177pp., <http://dx.doi.org/10.25607/OBP-432>.

WSR-88D Radar Operations Center, 2022: Interface Control Document for the RDA/RPG. NWS Doc. 2620002V, Build 21.0, 113 pp., <https://www.roc.noaa.gov/WSR88D/PublicDocs/ICDs/2620002V.pdf>

WSR-88D Radar Operations Center, 2020: Software Requirements Specification for the Radar Product Generator (SRS, CPCI-03). NWS Doc. 2820003N Pt. 1, Build 19.0, 205 pp.